

Structural Phase Transformations during a Solid-State Reaction in a Bilayer Al/Fe Thin-Film Nanosystem

R. R. Altunin^{a,*}, E. T. Moiseenko^a, and S. M. Zharkov^{a,b}

^a Siberian Federal University, Krasnoyarsk, 660041 Russia

^b Kirensky Institute of Physics, Federal Research Center Krasnoyarsk Science Center, Siberian Branch, Russian Academy of Sciences, Krasnoyarsk, 660036 Russia

*e-mail: raltunin@gmail.com

Received June 26, 2019; revised August 20, 2019; accepted August 20, 2019

Abstract—The processes of phase formation during a solid-state reaction between Fe and Al nanolayers have been investigated by the in situ electron diffraction method. It is established that the solid-state reaction at the interface between iron and aluminum nanolayers begins at $\approx 100^\circ\text{C}$ with the formation of a disordered Al solid solution in $\alpha\text{-Fe}$. It is shown that intermetallic phases (FeAl_6 and/or Fe_2Al_5 , FeAl , and Fe_3Al) are successively formed upon further heating.

Keywords: thin films, Al/Fe, solid-state reaction, phase formation, electron diffraction

DOI: 10.1134/S1063783420010059

1. INTRODUCTION

Compounds with aluminum are of great interest in various fields of application due to a favorable combination of physicochemical properties (for example, good resistance to oxidation at high temperatures and wear resistance) and low production cost [1, 2]. Thin-film systems based on Al and Fe are promising as heat- and corrosion-resistant coatings [3], metallization layers in microelectronics [4], materials for high-density magnetic data recording [5, 6], and reaction nanofilms for various purposes [7–12].

Investigations of solid-state reactions in thin-film systems are of not only practical but also fundamental importance. The processes of solid-state reactions occurring in thin films and bulk samples differ significantly. Solid-state reactions in thin-film systems can run at lower temperatures, as compared with bulk samples [13]. One of the most modern theoretical models, predicting not only the formation of the first phase, but also a sequence of phase formations during a solid-state reaction, is the effective heat of formation (EHF) model [14]. However, the use of this model for an Al/Fe thin-film system is difficult, because calculation of the effective phase-formation heats for Fe_2Al_5 , FeAl_6 , $\text{Fe}_4\text{Al}_{13}$, FeAl_2 , and FeAl_3 yields almost identical values, which makes it impossible to predict the phase sequence in this system. The application of a modified effective heat of formation (MEHF) model for this system also cannot solve the problem of predicting the phase sequence [15].

Note that experimental investigations of the phase sequence in a Al/Fe system do not give unambiguous results. It was reported in [16, 17] that the FeAl_6 metastable phase is the first to be formed during the solid-state reaction, which contradicts the data of [18, 19], in which the Fe_2Al_5 stable phase was first recorded. Different onset temperatures of the reaction between the iron and aluminum layers were reported in different experimental studies; e.g., the solid-state reaction beginning was observed at a temperature of 250°C in [17, 20], 300°C in [16, 18], and 350°C in [19].

The purpose of this study was to determine the initiation temperature of the solid-state reaction and establish the sequence of formation of intermetallic phases formed during the solid-state reaction in a Al/Fe thin-film system. The investigation was performed by the in situ electron diffraction method, which made it possible to investigate in detail both the initial stage of the solid-state reaction and the high-temperature region.

2. EXPERIMENTAL

Bilayer Al/Fe thin-film nanosystems investigated in this study were obtained using an MED-020 high-vacuum system (Bal-Tec) by electron-beam evaporation (residual pressure 5×10^{-5} Pa). The substrates were kept at room temperature during the deposition. High-purity materials were used for the deposition: Fe (99.9%) and Al (99.999%) [21]. The film thickness during the deposition was controlled with a QSG-100 quartz crystal thickness monitor (the accuracy in

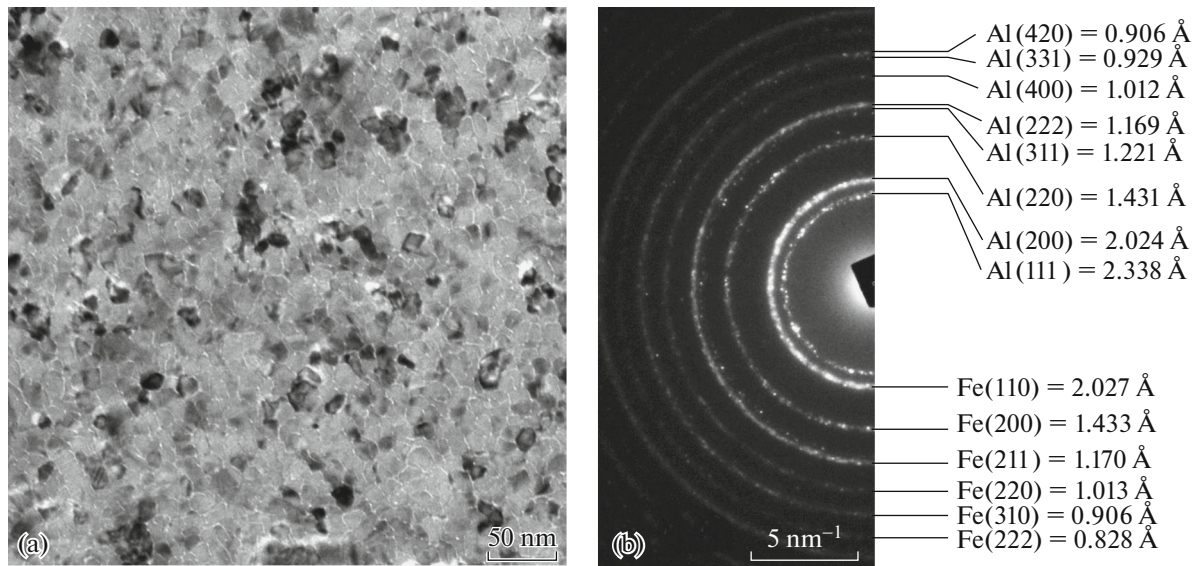


Fig. 1. (a) Electron microscopy image and (b) electron diffraction pattern recorded for the Al/Fe thin-film nanosystem in the initial state.

determining the integral film thickness was 0.01 nm). The iron and aluminum layers were successively deposited on a substrate (freshly cleaved NaCl single crystal). To carry out in situ electron microscopy analysis, the films deposited on NaCl were separated from the substrate in distilled water and then placed on an electron microscopy object grid made of molybdenum.

The microstructure and phase and elemental compositions were investigated on a JEOL JEM-2100 transmission electron microscope equipped with an Oxford Inca X-Sight energy-dispersive spectrometer. The films were heated directly in the transmission electron microscope column using a special sample holder designed for heating from room temperature to +1000°C. This method was successfully applied for studying structural phase transformations occurring during solid-state reactions in thin-film nanosystems: Al/Au [22], Cu/Au [23], Fe/Pd [23–25], Fe/Si [26], Fe-ZrO₂ [27], Co-ZrO₂ [28], and Al/Pt [29].

The phase composition of the samples under study was determined based on electron diffraction patterns recorded by the microdiffraction method from regions with a diameter of ≈ 1.3 μm . The electron diffraction patterns were analyzed using the CrystBox [30], Digital Micrograph [31], and Process Diffraction [32] software packages and the crystal structure database ICDD PDF 4+ [33].

3. RESULTS AND DISCUSSION

To perform electron microscopy studies, we prepared a series of bilayer Al/Fe thin-film nanosystems (atomic ratio Al : Fe $\approx 1 : 1$). The total thickness of the bilayer nanosystem was ≈ 50 nm. The individual-

nanolayer thicknesses were chosen so as to provide the above atomic ratio. The Fe and Al layer thicknesses were ≈ 20 and ≈ 30 nm, respectively.

An analysis of the elemental composition performed by energy-dispersive spectroscopy showed that the component contents in the samples obtained are 50 ± 0.5 at % Fe and 50 ± 0.5 at % Al. An analysis of the electron microscopy images (Fig. 1a) and electron diffraction patterns (Fig. 1b) recorded on the samples in the initial state showed that the thin-film nanosystems consist of α -Fe (sp. gr. *Im-3m*, lattice parameter $a = 2.866$ Å, PDF 4+ card no. 00-006-0696) and Al (sp. gr. *Fm-3m*, lattice parameter $a = 4.049$ Å, PDF 4+ card no. 00-004-0787) crystallites. Fe and Al crystallites were 10–20 nm in size. A complete set of diffraction reflections of the polycrystalline type corresponding to bcc α -Fe lattice and fcc Al lattice can be observed in the electron diffraction pattern (see Fig. 1b).

To study the processes of phase formation during the solid-state reaction between the Fe and Al nanolayers, the obtained Al/Fe thin-film nanosystems were heated with a rate of 8°C/min from room temperature to 850°C. During the sample heating, electron diffraction patterns were recorded with a rate of 4 frames/min (i.e., one frame corresponded to a change in the sample temperature by 2°C). This made it possible to determine the solid-state reaction initiation temperature, investigate the dynamics and processes of formation of solid solutions, and establish the sequence of phase formation during the solid-state reaction.

In the temperature range of 250–402°C, the electron diffraction patterns exhibited formation of weak spot crystalline reflections. An analysis of the electron

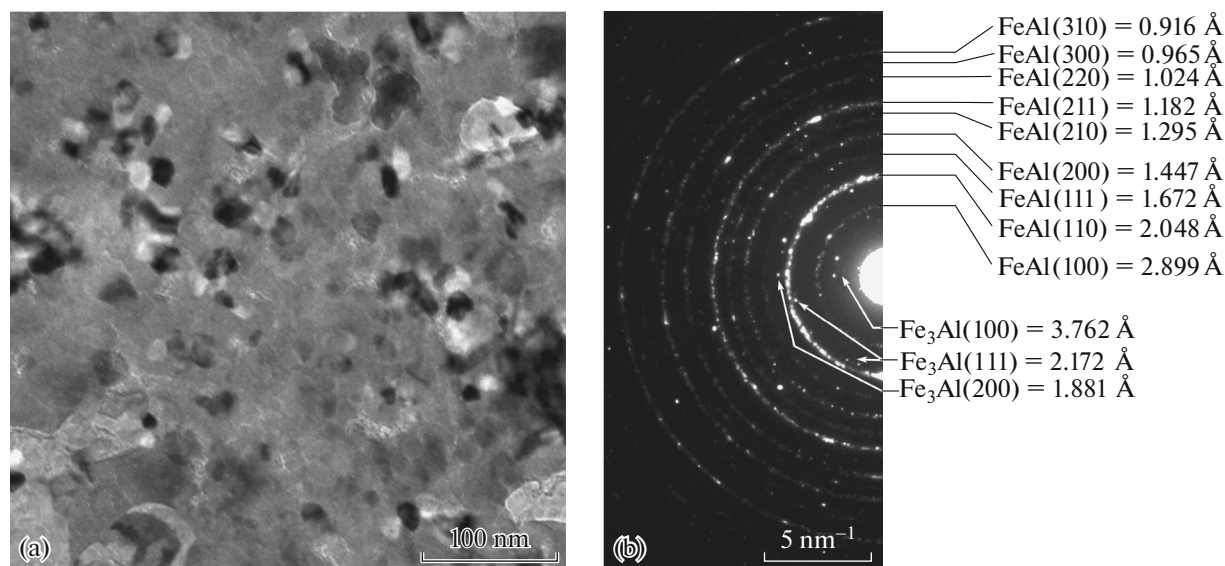


Fig. 2. (a) Electron microscopy image and (b) electron diffraction pattern recorded for the Al/Fe thin-film nanosystem after heating to 850°C.

diffraction patterns suggests that the observed reflections belong to intermetallic Al–Fe compounds. However, the specific intermetallic Al–Fe phase (or phases) cannot be exactly identified because of the insufficient number of the observed reflections and their low intensity.

In the temperature range of 404–669°C, spot diffraction reflections were observed in the electron diffraction patterns, which can be assigned to either the FeAl_6 phase (sp. gr. $Ccm21$, lattice parameters $a = 7.440 \text{ \AA}$, $b = 8.779 \text{ \AA}$, $c = 6.464 \text{ \AA}$, PDF 4+ card no. 04-007-0980) or the Fe_2Al_5 phase (sp. gr. $Cmcm$ (63), lattice parameters $a = 6.413 \text{ \AA}$, $b = 7.649 \text{ \AA}$, $c = 4.216 \text{ \AA}$, PDF 4+ card no. 00-047-1435). However, since the interplanar spacings that are characteristic of the FeAl_6 and Fe_2Al_5 phases are close, these reflections are difficult to interpret. An analysis of the electron diffraction patterns showed that intermetallic compounds in this stage of the solid-state reaction are formed as individual crystallites 30–40 nm in size.

Beginning of the formation of the FeAl phase (sp. gr. $Pm-3m$, lattice parameter $a = 2.895 \text{ \AA}$, PDF 4+ card no. 00-033-0020) was observed at 480°C, which was accompanied by the occurrence of ring reflections in the electron diffraction pattern that are typical of this phase. After achieving a temperature of 671°C, the electron diffraction patterns exhibited spot diffraction reflections that are characteristic of the Fe_3Al phase (sp. gr. $Pm-3m$, lattice parameter $a = 3.762 \text{ \AA}$, PDF 4+ card no. 04-005-9518).

An analysis of the electron microscopy images (Fig. 2a) and electron diffraction patterns (Fig. 2b) recorded on the sample after heating to 850°C showed that the sample consists of FeAl phase crystallites 20–

40 nm in size and scarce individual Fe_3Al phase crystallites 30–50 nm in size. The analysis of the electron diffraction patterns using the Process Diffraction software package [32] showed that, after the heating, the amount of the Fe_3Al phase in the film is $\approx 2.2 \text{ vol } \%$.

An analysis of the diffraction reflections in the electron diffraction patterns recorded after heating to 400°C showed that the diameters of all the observed ring reflections decrease during the heating. This fact indicates that the lattice parameters of aluminum and iron change with the lattice type remained the same. Note that the majority of the diffraction reflections of the fcc aluminum and bcc iron phases almost coincide (e.g., Al $d(200) = 2.024 \text{ \AA}$ and Fe $d(110) = 2.027 \text{ \AA}$), which hinders determination of the lattice parameters for fcc aluminum and bcc iron. In the case of fcc aluminum, there is a characteristic (111) reflection (not coinciding with bcc iron reflections), which was used to calculate the change in the lattice parameter of fcc aluminum upon heating. The bcc iron lattice parameter was calculated based on analyzing the position of the $\alpha\text{-Fe}$ (110) reflection, which coincides with the Al(200) reflection, but is much stronger.

Figures 3a and 3b show the changes in the lattice parameters for Al and $\alpha\text{-Fe}$ upon heating the films to 400°C. Curves I and II in Fig. 3a (3b) are the temperature dependences of the lattice parameter for Al ($\alpha\text{-Fe}$) with the linear thermal expansion coefficient (LTEC) neglected and taken into account, respectively.

An analysis of the changes in the lattice parameter of $\alpha\text{-Fe}$ upon heating (Fig. 3b, curve II) shows that the iron lattice parameter begins to increase at $\approx 100^\circ\text{C}$, whereas the aluminum lattice parameter remains constant (within the measurement error) up to $\approx 250^\circ\text{C}$

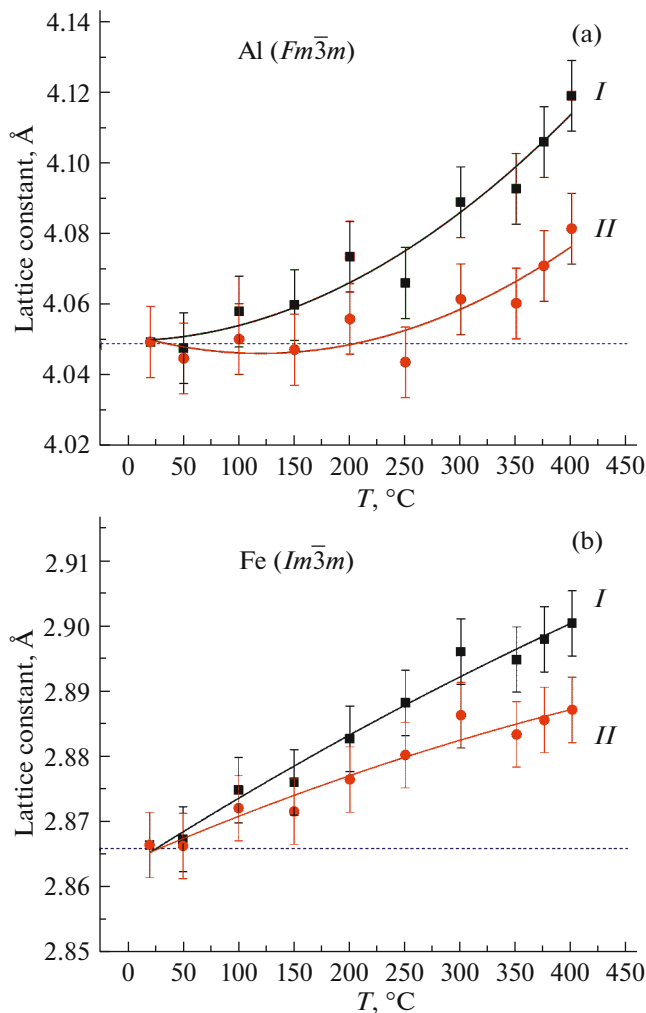


Fig. 3. Changes in the lattice constant for (a) aluminum and (b) iron upon heating of the Al/Fe thin-film nanosystem to 400°C with the LTEC (curves *I*) neglected and (curves *II*) taken into account.

(Fig. 3a, curve *II*). This fact indicates that a disordered Al solid solution in α -Fe with the bcc lattice is formed in the film even at 100°C. According to the data of [34], the observed change in the lattice parameter of α -Fe (Fig. 3b, curve *II*) from 2.866 Å (initial state) to 2.886 Å (300°C) corresponds to a Fe(Al) solid solution containing ≈ 8 at % Al.

An analysis of the change in the aluminum lattice parameter (Fig. 3a, curve *II*) at $T > 250^\circ\text{C}$ suggests that the observed increase in the lattice parameter is not real and related to the formation of intermetallic phases rather than Al(Fe) solid solution. According to the data of [34], formation of the Al(Fe) solid solution should be accompanied by a decrease (rather than increase) in the aluminum lattice parameter. In this study, intermetallic Al–Fe compounds are formed as individual crystallites in the initial stage (250–402°C) of the solid-state reaction, which is accompanied by

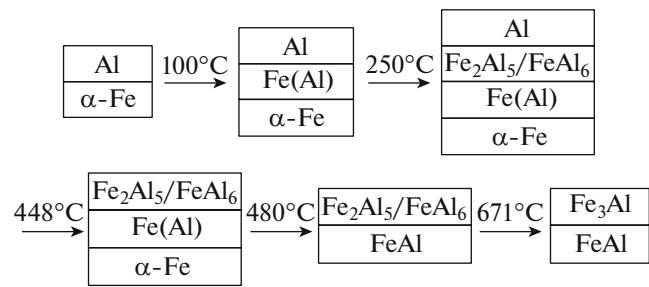
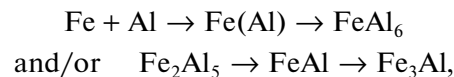


Fig. 4. Schematic of the phase-formation sequence during the solid-state reaction in the Al/Fe thin-film nanosystem.

the occurrence of point reflections with $d = 2.35$ – 2.37 Å in the electron diffraction patterns. Since the aluminum lattice parameter is calculated in this study from the Al $d(111) = 2.34$ Å reflection, the occurrence of intermetallic-phase reflections leads to the apparent increase in the aluminum lattice parameter. In works [16–18] devoted to bilayer Al/Fe films, the beginning of the solid-state reaction was accompanied by the formation of FeAl₆ and/or Fe₂Al₅ intermetallic compounds at 250–330°C. We can suggest that, in this study, the FeAl₆ and/or Fe₂Al₅ phases are formed in the temperature range of 250–402°C in a small volume at the aluminum–iron nanolayer interface.

Proceeding from the performed investigations of phase formation during the solid-state reaction in Al/Fe thin-film nanosystems (atomic ratio Al : Fe $\approx 1 : 1$), we proposed the following phase-formation sequence:



which is shown schematically in Fig. 4.

The temperature regions of existence of intermetallic compounds that are formed during the solid-state reaction in the Al/Fe thin-film nanosystem are given in Table 1.

According to the EHF model [14], the phase with the least effective formation heat $\Delta H'$ is the first to be formed during the solid-state reaction. Formation heats ΔH^0 and effective formation heats $\Delta H'$ for the Fe–Al phases are listed in Table 2. The ΔH^0 and $\Delta H'$ values for the Fe₃Al, FeAl₂, Fe₂Al₅, FeAl₃, and FeAl₆ phases were taken from [14]. Formation heat ΔH^0 of the FeAl and Fe₄Al₁₃ phases was calculated using the data of [35]. Effective formation heat $\Delta H'$ was calculated based on the obtained ΔH^0 value.

According to Table 2, the Fe₂Al₅, FeAl₆, Fe₄Al₁₃, FeAl₂, and FeAl₃ phases have the least effective formation heats. Moreover, the values of the effective formation heats of these phases differ only slightly (by 0.01 kJ (mol atom)⁻¹). This means that these phases should be formed almost simultaneously during the solid-state reaction. However, this situation is not

Table 1. Structural phase transformations in Al/Fe thin-film nanosystem during the solid-state reaction initiated by thermal heating with a rate of 8°C/min

$T, ^\circ\text{C}$	Al	$\alpha\text{-Fe}$	Fe(Al) solid solution	FeAl ₆ Fe ₂ Al ₅	FeAl	Fe ₃ Al
25–98	+	+				
100–248	+	+	+			
250–402	+	+	+	?		
404–446	+	+	+	+		
448–478		+	+	+		
480–669		?	?	+	+	
671–850		?	?		+	s

Symbol “s” indicates that the amount of the phase in the film is small (<10 wt %). Symbol “?” indicates that the phase may be present.

Table 2. Values of formation heat ΔH^0 and effective formation heat $\Delta H'$ for Al–Fe phases

Phase	Formation Heat ΔH^0 , kJ (mol atom) ⁻¹	Effective formation heat $\Delta H'$, kJ (mol atom) ⁻¹	References
FeAl ₆	–11	–0.69	[14]
Fe ₂ Al ₅	–22	–0.69	[14]
Fe ₄ Al ₁₃	–18	–0.69	[35]
FeAl ₂	–25	–0.68	[14]
FeAl ₃	–19	–0.68	[14]
FeAl	–32	–0.58	[35]
Fe ₃ Al	–22	–0.26	[14]

consistent with the experimental results obtained by us and other researchers [16–18]. The successive phase formation FeAl (–0.58 kJ (mol atom)⁻¹) → Fe₃Al (–0.26 kJ (mol atom)⁻¹), observed in this study, is in agreement with the EHF model. It should be noted that the Fe₃Al phase formation in thin-film systems was previously only suggested to occur proceeding from an analysis of the magnetic properties [36] and the presence of this phase was not confirmed by direct structural methods. It was shown in this study by the in situ electron diffraction method that the Fe₃Al phase is formed at a temperature of 671°C during the solid-state reaction between the Fe and Al nanolayers.

4. CONCLUSIONS

The processes of phase formation during the solid-state reaction between Fe and Al nanolayers (atomic ratio Al : Fe ≈ 1 : 1, individual-layer thickness 20–30 nm) were investigated. The solid-state reaction was

initiated by thermal heating in the transmission electron microscope column. The reaction initiation temperature and the sequence of phase formations were determined based on the data obtained by the in situ electron diffraction method directly during the solid-state reaction. It was established that the solid-state reaction at the interface between the aluminum and iron nanolayers begins (at ≈100°C) with the formation of a disordered Al solid solution in $\alpha\text{-Fe}$. It was shown that the FeAl₆ and/or Fe₂Al₅, FeAl, and Fe₃Al intermetallic phases are successively formed upon further heating. The Fe₃Al phase formation during the solid-state reaction in an Al/Fe thin-film nanosystem was observed for the first time using a direct structural method.

FUNDING

This study was supported by the Russian Foundation for Basic Research, project no. 18-03-01173a.

CONFLICT OF INTEREST

The authors declare that they have no conflicts of interest.

REFERENCES

- H. Y. Gao, Y. H. He, P. Z. Shen, Y. Jiang, and C. T. Liu, *Adv. Powder Technol.* **26**, 882 (2015).
- Y. Liu, X. Chong, Y. Jiang, R. Zhou, and J. Feng, *Phys. B (Amsterdam, Neth.)* **506**, 1 (2017).
- M. Palm, *Int. J. Mater. Res.* **100**, 277 (2009).
- P. Mengucci, G. Majni, A. di Cristoforo, R. Checchetto, A. Miotello, C. Tosello, and G. Principi, *Thin Solid Films* **433**, 205 (2003).
- T. Abe, T. Kawai, M. Futamoto, M. Ohtake, and N. Inaba, *AIP Adv.* **8** (2018).
- Y. Wei, W. Shao, Z. Ma, Z. Chen, and W. Lu, *Mater. Lett.* **185**, 537 (2016).
- A. S. Rogachev, *Russ. Chem. Rev.* **77**, 21 (2008).
- V. G. Myagkov, V. S. Zhigalov, L. E. Bykova, and V. K. Mal'tsev, *Tech. Phys.* **43**, 1189 (1998).
- A. S. Rogachev, S. G. Vadchenko, A. A. Nepapushev, and A. S. Mukasyan, *Int. J. Self-Propag. High-Temp. Synth.* **25**, 234 (2016).
- D. J. Fisher, *Bonding by Self-Propagating Reaction* (Mater. Res. Forum, Millersville, PA, 2019).
- R. Checchetto, C. Tosello, A. Miotello, and G. Principi, *J. Phys.: Condens. Matter* **13**, 811 (2001).
- S. Jani, V. Sebastian, N. Lakshmi, V. R. Reddy, K. Venugopalan, A. Gupta, and N. P. Lalla, *J. Appl. Phys.* **104**, 123907 (2008).
- J. M. Poate, K. N. Tu, and J. W. Mayer, *Thin Films—Interdiffusion and Reactions* (Wiley, New York, 1982).
- R. Pretorius, T. Marais, and C. Theron, *Mater. Sci. Rep.* **10**, 1 (1993).
- K. Bhanumurthy, W. Krauss, and J. Konys, *Fusion Sci. Technol.* **65**, 262 (2014).

16. F. Haidara, M.-C. Record, B. Duployer, and D. Mangelinck, *Intermetallics* **23**, 143 (2012).
17. A. Csanády, J. R. Günter, P. B. Barna, and J. Mayer, *Thin Solid Films* **167**, 203 (1988).
18. S. R. Teixeira, F. L. Freire, and I. J. R. Baumvol, *Appl. Phys. A* **48**, 481 (1989).
19. P. Bhattacharya, K. N. Ishihara, and K. Chattopadhyay, *Mater. Sci. Eng. A* **304–306**, 250 (2001).
20. J. L. Alexandre, M. A. Z. Vasconcellos, S. R. Teixeira, and I. J. R. Baumvol, *Appl. Phys. A* **56**, 113 (1993).
21. ADVENT Research Materials Ltd., Oxford, UK. www.advent-rm.com.
22. R. R. Altunin and S. M. Zharkov, *Bull. Russ. Acad. Sci.: Phys.* **77**, 1004 (2013).
23. S. M. Zharkov, E. T. Moiseenko, and R. R. Altunin, *J. Solid State Chem.* **269**, 36 (2019).
24. S. M. Zharkov, E. T. Moiseenko, R. R. Altunin, N. S. Nikolaeva, V. S. Zhigalov, and V. G. Myagkov, *JETP Lett.* **99**, 405 (2014).
25. E. T. Moiseenko, R. R. Altunin, and S. M. Zharkov, *Phys. Solid State* **59**, 1233 (2017).
26. S. M. Zharkov, R. R. Altunin, E. T. Moiseenko, G. M. Zeer, S. N. Varnakov, and S. G. Ovchinnikov, *Solid State Phenom.* **215**, 144 (2014).
27. V. G. Myagkov, L. E. Bykova, O. A. Bayukov, V. S. Zhigalov, I. A. Tambasov, S. M. Zharkov, A. A. Matsynin, and G. N. Bondarenko, *J. Alloys Compd.* **636**, 223 (2015).
28. V. G. Myagkov, V. S. Zhigalov, L. E. Bykova, S. M. Zharkov, A. A. Matsynin, M. N. Volochaev, I. A. Tambasov, and G. N. Bondarenko, *J. Alloys Compd.* **665**, 197 (2016).
29. R. R. Altunin, E. T. Moiseenko, and S. M. Zharkov, *Phys. Solid State* **60**, 1413 (2018).
30. M. Klinger and A. Jäger, *J. Appl. Crystallogr.* **48**, 2012 (2015).
31. Gatan Inc., Digital Micrograph (Pleasanton, CA, 2007).
32. J. L. Lábár, *Proc. Eurem* **12**, 379 (2000).
33. *Powder Diffraction File (PDF 4+, 2018)*, *Inorganic Phases* (Int. Center for Diffraction Data, Swarthmore, PA, USA, 2018).
34. *Landolt-Börnstein, New Ser., Group IV*, Ed. by B. Preidel and O. Madelung (Springer, 1991), Vol. 5A.
35. A. Debski, R. Debski, and W. Gasior, *Arch. Metall. Mater.* **59**, 1337 (2014).
36. R. Brajpuria, *Surf. Interface Anal.* **50**, 1349 (2018).

Translated by A. Sin'kov